Hindawi
Advances in Civil Engineering
Volume 2018, Article ID 1490848, 10 pages
https://doi.org/10.1155/2018/1490848

Research Article

Upper Bound Solution of Surrounding Rock Pressure for Deep Cavity Using Nonlinear Hoek–Brown Failure Criterion

Cheng-yang Wang,[1] **He-lin Fu**,[2] **and Jun-zhe Liu**[3]

[1]*Ph.D., School of Civil Engineering, Central South University, Hunan 410075, China*
[2]*Professor, School of Civil Engineering, Central South University, Hunan 410075, China*
[3]*Institute of Mountain Hazards and Environment, Chinese Academy of Sciences, Chengdu 610000, China*

Correspondence should be addressed to Cheng-yang Wang; wangchengy@csu.edu.cn

Received 11 July 2018; Accepted 27 August 2018; Published 23 September 2018

Academic Editor: Dengke Wang

The linear failure criterion is generally adopted in the stability problem of geotechnical engineering, whereas the experiments have indicated that there is a nonlinear relationship between the maximum and minimum principal stresses in weak surrounding rock. According to the characteristics of weak rock, the failure mechanism of deep cavity is constructed by combining the nonlinear Hoek–Brown failure criterion and the upper bound theorem of limit analysis. The upper bound solution of the surrounding rock pressure was deduced using the tangent method. The results show that the surrounding rock pressure of deep cavity is affected by surrounding rock grade, cavity depth, and section size. Especially, the influence of the disturbance factor is quite obvious. Upper bound solution based on nonlinear Hoek–Brown failure criterion can fully take the influence of parameters on surrounding rock pressure. Therefore, this method is more scientific than the linear failure criterion to calculate the surrounding rock pressure.

1. Introduction

The stability problem of deep cavity has been highlighted greatly and continuously in the field of the underground engineering, whereas the problem that needs to be solved urgently is how to accurately obtain the surrounding rock pressure when the deep cavern is destroyed [1, 2]. Currently, the analytic methods for solving the surrounding rock pressure mainly include the limit equilibrium method and the limit analysis method, both of which have been illustrated widely in literature. However, the former does not consider the constitutive relationship of rock, while the latter does by adopting the orthogonal flow rule. Therefore, the upper bound theory is more rigorous than the limit equilibrium method. Especially, there is no need to study the whole process of rock's elastic-plastic deformation, but directly to pay attention to the ultimate failure state of rock. Thus, its calculation process is simple and has been regarded as one of the most effective approaches to solve the surrounding rock pressure problem in the deep cavity [3–5].

In recent years, some scholars have adopted the limit analysis method to study the surrounding rock pressure of deep cavity. According to the results of the model test, Davis et al. [6] proposed four failure mechanisms for underground cavity, which included the arch collapse mode and vault collapse mode bordered wall, and obtained the upper bound solution of the surrounding rock pressure by the limit analysis method. Takemura et al. [7] constructed the failure mechanism of the deep cavity using the centrifugal model test. The failure model is composed of 5 rigid blocks, and the limit analysis method is used to solve the surrounding rock pressure of the underground cavity under the anisotropic soil conditions. The results were compared with the measured values, and the validity of the results has been verified. Yang and Yang [8] proposed the destruction mechanism of underground chambers composed of n blocks. According to the requirement of calculation accuracy, the upper bound solution of surrounding rock pressure under different number of blocks was obtained. Through comparison, the destruction characteristics of deep cavity can be better

illustrated with more rigid blocks, and accordingly, the surrounding rock pressure is more accurate. However, the above research studies are applied to shallow buried cavity where the Mohr–Coulomb failure criterion is used and more suitable for soil mass.

For deep cavity, Atkinson and Potts [9] established the failure mode of circular which were based on the results of model tests, obtained the upper bound solution of the surrounding rock pressure using the limit analysis method, and the correctness of the results was verified. And the curve failure mechanism of the deep cavity based on the limit analysis method was proposed by Fraldi and Guarracino [10–12], which the Hoek–Brown failure criterion and the variational method were applied to solve the analytic expression of the curve and got the surrounding rock pressure under the limit state of the vault collapse. Yang and Yang [8] combined the limit analysis theory with the variational principle, deduced the expression of the surrounding rock pressure of deep rectangle cavity and specified the corresponding failure range. In addition, Huang et al. [13] took the influence of pore water based on the previous research studies into account and got a reasonable result. The limit analysis method was used to calculate the surrounding rock pressure of deep buried circular cavity. Compared with the existing research results, the correctness of the calculation results was verified. Qin et al. [2] considered the multilayer rock mass and used the upper bound method to study the influence of the variation of the parameters of the Hoek–Brown failure criterion on the surrounding rock pressure of the deep buried rectangular cavity. The vault of deep cavity was only considered and assumed to obey a curve function $f(x)$ in the abovementioned studies, and yet, the side wall was ignored in the analysis. However, it could not accord with the conditions in reality.

Therefore, by referring to the previous research results, the multiblock and logarithmic spiral curves are used to construct the failure mechanism of deep cavity in this paper. Based on the upper bound theorem of limit analysis and Hoek–Brown failure criterion, the vault and side wall damage state is investigated to determine the rock pressure when the deep cavity collapses and provide the scientific basis for the design in engineering.

2. Hoek–Brown Nonlinear Failure Criterion and Tangent Method

In 1980, Brown proposed the initial Hoek–Brown failure criterion on the basis of Hoek's experimental research studies on rock plastic behaviors. Subsequently, Hoek made a further revision to the failure criterion and put forward the modified generalized Hoek–Brown criterion. It is expressed as follows [14, 15]:

$$\sigma_1' = \sigma_3' + \sigma_{ci}\left(m_b\frac{\sigma_3'}{\sigma_{ci}} + S\right)^{\alpha}, \tag{1}$$

where σ_1' and σ_3' are the maximum and minimum effective principal stress of rock mass at critical failure, respectively; σ_{ci} is the uniaxial compressive strength of rock; α is the physical index relating to the integrity of rock; m_b and S indicate the dimensionless parameters related to geotechnical materials, which characterizes the integrity of the rock. The above parameters can be calculated through the GSI index; the specific process is as follows [16–18]:

$$\begin{aligned} m_b &= m_i \exp\left(\frac{\mathrm{GSI}-100}{28-14D}\right),\\ S &= \exp\left(\frac{\mathrm{GSI}-100}{9-3D}\right),\\ \alpha &= \frac{1}{2}+\frac{1}{6}+\left(e^{-\mathrm{GSI}/15}-e^{-20/3}\right). \end{aligned} \tag{2}$$

For the upper limit solution of the deep cavity under the Hoek–Brown failure criterion, it is necessary to use the tangent method to obtain the counterforce of the support. Among them, the correlations between c_t and φ_t can be written as follows [19, 20]:

$$\begin{aligned} \frac{c_t}{\sigma_{ci}} = \frac{\cos\varphi_t}{2}\left[\frac{ma\left(1-\sin\varphi_t\right)}{2\sin\varphi_t}\right]^{(a/1-a)} - \frac{\tan\varphi_t}{m}\left(1+\frac{\sin\varphi_t}{a}\right)\\ \cdot\left[\frac{ma\left(1-\sin\varphi_t\right)}{2\sin\varphi_t}\right]^{(a/1-a)} + \frac{s}{m}\tan\varphi_t. \end{aligned} \tag{3}$$

In the above formula, the nonlinear shear strength index φ_t can be optimized by the least energy principle when the upper bound is calculated. The c_t is obtained by Equation (3) after the determination of φ_t.

3. Building Destruction Mechanism

During the excavation process of the deep cavity, the collapse easily happens due to the untimely support or weak strength. Based on the existing research results [8, 10] and the requirement of the upper bound theorem of limit analysis, the failure mode of deep cavity was structured, as shown in Figure 1. The width of the chamber is l, and the height is h. The wedge $ABGOG_1B_1$ at the top of the cavity is collapsing vertically and downwards at a rate of v_0. The BGC and $B_1G_1C_1$ segments, respectively, rotate failure around G and G_1 points. The triangles CGD, DGE, and EGF and $C_1G_1D_1$, $D_1G_1E_1$, and $E_1G_1F_1$ would undergo translational failure. The surrounding rock pressure of vault and side wall are q and e, respectively, and $e = Kq$.

The velocity vector diagram corresponding to this failure mechanism is shown in Figure 2.

Calculation of speed and velocity discontinuity's length:

$$V_1 = V_0. \tag{4}$$

Based on the analysis of the velocity field in the shear zone of the circular arc radiation, the following can be obtained:

$$V_2 = V_1 \cdot e^{\alpha_1 \tan 2\varphi} = V_0 \cdot e^{\alpha_1 \tan 2\varphi}. \tag{5}$$

From Figure 2 and geometric triangle relationship can be obtained:

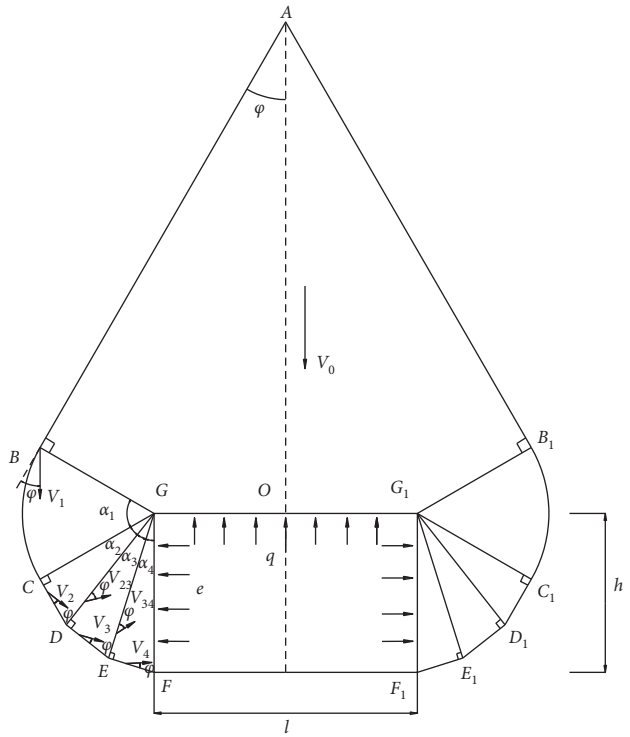

Figure 1: Diagrammatic sketch of circular sandwich failure mechanism.

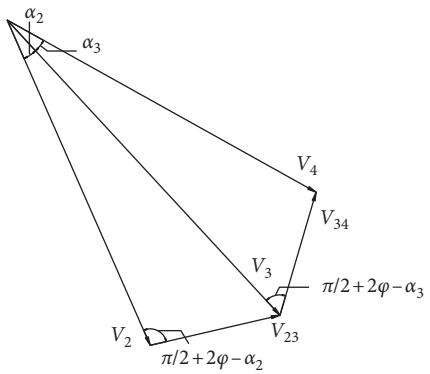

Figure 2: Velocity vector diagram.

$$
\begin{aligned}
V_{23} &= \frac{\sin\alpha_2}{\cos 2\varphi}V_2,\\
V_3 &= \frac{\cos(2\varphi-\alpha_2)}{\cos 2\varphi}V_2,\\
V_4 &= \frac{\cos(2\varphi-\alpha_3)}{\cos 2\varphi}V_3,\\
V_{34} &= \frac{\sin\alpha_3}{\cos 2\varphi}V_3.
\end{aligned}
\tag{6}
$$

The recurrence relation of various velocity discontinuities is as follows:

$$
\begin{aligned}
GE &= \cos\alpha_4 GF,\\
EF &= \sin\alpha_4 GF,\\
GD &= \cos\alpha_3 GE,\\
DE &= \sin\alpha_3 GE,\\
GC &= \cos\alpha_2 GD,\\
CD &= \sin\alpha_2 GD,\\
GB &= GC,\\
AO &= AB\cdot\cos\varphi + BG\cdot\sin\varphi,\\
AB &= \frac{BG}{\tan\varphi}+\frac{GO}{\sin\varphi},\\
&\begin{cases} GO = \dfrac{l}{2},\\ GF = h. \end{cases}
\end{aligned}
\tag{7}
$$

4. Calculation of Surrounding Rock Pressure

According to the upper bound theorem of limit analysis, the external power and internal energy dissipation rate can be obtained when the deep cavity collapses. If the external power and internal energy dissipation rate are equal, the surrounding rock pressure at the collapse of the deep cavity can be obtained.

4.1. Calculation of External Power

4.1.1. Power of Gravity. Area of each rigid block:

$$
\begin{aligned}
\frac{1}{2}S_{ABGOG_1B_1} &= S_{ABGO} = \frac{1}{2}BG\cdot AB+\frac{1}{2}AO\cdot GO,\\
S_{GBC} &= \int_0^{\alpha_1}\frac{1}{2}GB^2 d\theta',\\
S_{GCD} &= \frac{1}{2}GC\cdot CD,\\
S_{GDE} &= \frac{1}{2}GD\cdot DE,\\
S_{GEF} &= \frac{1}{2}GE\cdot EF.
\end{aligned}
\tag{8}
$$

The gravitational power generated by each rigid slider is as follows.

Quadrilateral rigid block *ABGO*:

$$W_1 = \gamma \cdot S_{ABGO} \cdot V_0 = \gamma \cdot \left(\frac{1}{2} BG \cdot AB + \frac{1}{2} AO \cdot GO\right) \cdot V_0 = \gamma \cdot V_0 \cdot h^2 \cdot f_1,$$

$$f_1 = \frac{1}{2}\cos\alpha_2 \cos\alpha_3 \cos\alpha_4 \cdot \left(\frac{\cos\alpha_2 \cos\alpha_3 \cos\alpha_4}{\tan\varphi} + \frac{l}{2h\sin\varphi}\right) + \left[\left(\frac{\cos\alpha_2 \cos\alpha_3 \cos\alpha_4}{\tan\varphi} + \frac{l}{2h\sin\varphi}\right) \cdot \cos\varphi + \cos\alpha_2 \cos\alpha_3 \cos\alpha_4 \cdot \sin\varphi\right] \cdot \frac{l}{4h}. \tag{9}$$

Sector region *GBC*:

The power calculation of circular shear zone *BGC* is shown in Figure 3.

$$W_2 = \gamma \int_0^{\alpha_1} \frac{1}{2} \cdot GB^2 \cdot d\theta' \cdot V_0 e^{\theta' \tan 2\varphi} \sin\left(\frac{\pi}{2} - \theta'\right) = \gamma \cdot V_0 \cdot h^2 \cdot f_2. \tag{10}$$

Among them,

$$f_2 = \frac{1}{2} \cdot \frac{\cos^2\alpha_2 \cos^2\alpha_3 \cos^2\alpha_4}{1 + \tan^2 2\varphi} \cdot \left[(\sin\alpha_1 + \tan 2\varphi \cos\alpha_1) e^{\alpha_1 \tan 2\varphi} - \tan 2\varphi\right]. \tag{11}$$

Triangular rigid block *GCD*:

$$W_3 = \gamma S_{GCD} V_2 \cos\left(\frac{\pi}{2} + \varphi - \alpha_2 - \alpha_3 - \alpha_4\right) = \gamma \cdot \frac{1}{2} GC \cdot CD \cdot V_2 \cdot \sin(\alpha_2 + \alpha_3 + \alpha_4 - \varphi) = \gamma h^2 V_0 f_3. \tag{12}$$

Among them,

$$f_3 = \frac{1}{2}\sin\alpha_2 \cdot \cos\alpha_2 \cdot \cos^2\alpha_3 \cdot \cos^2\alpha_4 \cdot \sin(\alpha_2 + \alpha_3 + \alpha_4 - \varphi) \cdot e^{\alpha_1 \tan 2\varphi}. \tag{13}$$

Triangular rigid block *GDE*:

$$W_4 = \gamma \cdot S_{GDE} \cdot V_3 \cdot \cos\left(\frac{\pi}{2} + \varphi - \alpha_1 - \alpha_2\right) = \gamma \cdot \frac{1}{2} GD \cdot DE \cdot V_3 \cdot \sin(\alpha_3 + \alpha_4 - \varphi) = \gamma h^2 V_0 f_4. \tag{14}$$

Among them,

$$f_4 = \frac{1}{2}\sin\alpha_3 \cdot \cos\alpha_3 \cdot \cos^2\alpha_4 \cdot \frac{\cos(2\varphi - \alpha_2)}{\cos 2\varphi} \cdot e^{\alpha_1 \tan 2\varphi} \cdot \sin(\alpha_3 + \alpha_4 - \varphi). \tag{15}$$

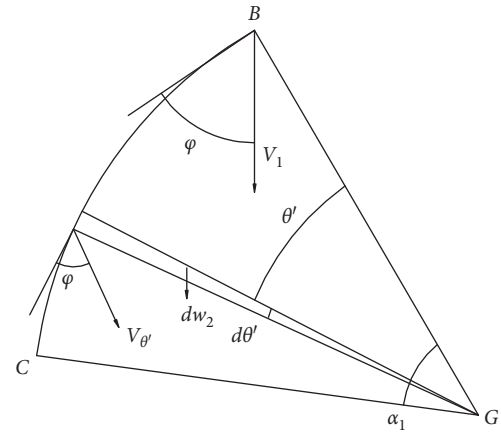

Figure 3: Schematic diagram of the power calculation of circular shear zone *BGC*.

Triangular rigid block *GEF*:

$$W_5 = \gamma \cdot S_{GEF} \cdot V_4 \cdot \cos\left(\frac{\pi}{2} + \varphi - \alpha_4\right) = \gamma \cdot \frac{1}{2} GE \cdot EF \cdot V_4 \cdot \sin(\alpha_4 - \varphi) = \gamma h^2 V_0 f_5. \tag{16}$$

Among them,

$$f_5 = \frac{1}{2}\sin\alpha_4 \cdot \cos\alpha_4 \cdot \frac{\cos(2\varphi - \alpha_3) \cdot \cos(2\varphi - \alpha_2)}{\cos^2 2\varphi} e^{\alpha_1 \tan 2\varphi} \cdot \sin(\alpha_4 - \varphi). \tag{17}$$

Power of gravity:

$$W_{\text{soil}} = \gamma h^2 V_0 (f_1 + f_2 + f_3 + f_4 + f_5). \tag{18}$$

4.1.2. Power of Supporting Force.

$$W_T = -q \cdot \frac{l}{2} \cdot V_0 - e \cdot h \cdot V_4 \cdot \sin(\alpha_4 - \varphi), = -q \cdot \frac{l}{2} \cdot V_0 - Kq \cdot h \cdot \frac{\cos(2\varphi - \alpha_3) \cdot \cos(2\varphi - \alpha_2)}{\cos^2 2\varphi} e^{\alpha_1 \tan 2\varphi} \cdot V_0 \cdot \cos(\alpha_4 - \varphi), = -qV_0 h f_6. \tag{19}$$

Among them,

$$e = Kq,$$

$$f_6 = \frac{l}{2h} + K \cdot \frac{\cos(2\varphi - \alpha_3) \cdot \cos(2\varphi - \alpha_2)}{\cos^2 2\varphi} e^{\alpha_1 \tan 2\varphi} \cdot \cos(\alpha_4 - \varphi). \tag{20}$$

4.1.3. Total External Power. The total external power is equal to the sum of the deadweight power of the surrounding rock and the power of the supporting counterforce. That is,

$$W_{\text{ext}} = W_{\text{soil}} + W_T = \gamma h^2 V_0 (f_1 + f_2 + f_3 + f_4 + f_5) - qhV_0 f_6. \tag{21}$$

4.2. Internal Energy Dissipation Power. Energy dissipation along discontinuity line *AB*:

$$D_{AB} = c \cdot AB \cdot V_0 \cdot \cos\varphi = \left(\frac{h \cdot \cos\alpha_2 \cdot \cos\alpha_3 \cdot \cos\alpha_4}{\tan\varphi} + \frac{l}{2\sin\varphi}\right) \cdot c \cdot V_0 \cdot \cos\varphi = c \cdot V_0 \cdot h \cdot f_7. \tag{22}$$

Among them,

$$f_7 = \left(\frac{\cos\alpha_2 \cdot \cos\alpha_3 \cdot \cos\alpha_4}{\tan\varphi} + \frac{l}{2h\sin\varphi}\right) \cdot \cos\varphi. \tag{23}$$

Energy dissipation of circular shear surface *BC* and shear zone *GBC*:

$$D_{BC} = \frac{c \cdot BG \cdot V_1 \cdot \cos\varphi}{\tan 2\varphi}\left(e^{\alpha_1 \cdot \tan 2\varphi} - 1\right) = chV_0 f_8,$$
$$f_8 = \frac{\cos\alpha_4 \cos\alpha_3 \cos\alpha_2 \cdot \cos\varphi}{\tan 2\varphi}\left(e^{\alpha_1 \cdot \tan 2\varphi} - 1\right),$$
$$D_{GBC} = \frac{c \cdot BG \cdot V_1 \cdot \cos\varphi}{\sin 2\varphi}\left(e^{\alpha_1 \cdot \tan 2\varphi} - 1\right) = chV_0 f_9,$$
$$f_9 = \frac{\cos\alpha_4 \cos\alpha_3 \cos\alpha_2 \cdot \cos\varphi}{\sin 2\varphi}\left(e^{\alpha_1 \cdot \tan 2\varphi} - 1\right). \tag{24}$$

Energy dissipation along discontinuity line *CD*:

$$D_{CD} = c \cdot CD \cdot V_2 \cdot \cos\varphi = chV_0 f_{10},$$
$$f_{10} = \sin\alpha_2 \cos\alpha_3 \cos\alpha_4 \cdot e^{\alpha_1 \tan 2\varphi} \cdot \cos\varphi. \tag{25}$$

Energy dissipation along discontinuity line *GD*:

$$D_{GD} = c \cdot GD \cdot V_{23} \cdot \cos\varphi = chV_0 f_{11},$$
$$f_{11} = \frac{\sin\alpha_2 \cos\alpha_3 \cos\alpha_4 \cos\varphi}{\cos 2\varphi} e^{\alpha_1 \tan 2\varphi}. \tag{26}$$

Energy dissipation along discontinuity line *DE*:

$$D_{DE} = c \cdot DE \cdot V_3 \cdot \cos\varphi = chV_0 f_{12},$$
$$f_{12} = \frac{\cos(2\varphi - \alpha_2)\sin\alpha_3 \cos\alpha_4 \cos\varphi}{\cos 2\varphi} e^{\alpha_1 \tan 2\varphi}. \tag{27}$$

Energy dissipation along discontinuity line *GE*:

$$D_{GE} = c \cdot GE \cdot V_{34} \cdot \cos\varphi = chV_0 f_{13},$$
$$f_{13} = \frac{\cos\varphi \cos\alpha_4 \sin\alpha_3 \cos(2\varphi - \alpha_2)}{\cos^2 2\varphi} e^{\alpha_1 \tan 2\varphi}. \tag{28}$$

Energy dissipation along discontinuity line *EF*:

$$D_{EF} = c \cdot EF \cdot V_4 \cdot \cos\varphi = chV_0 f_{14},$$
$$f_{14} = \frac{\sin\alpha_4 \cos\varphi \cos(2\varphi - \alpha_3)\cos(2\varphi - \alpha_2)}{\cos^2 2\varphi} e^{\alpha_1 \tan 2\varphi}. \tag{29}$$

Total internal energy dissipation:

$$D_{\text{int}} = chV_0 \cdot (f_7 + f_8 + f_9 + f_{10} + f_{11} + f_{12} + f_{13} + f_{14}). \tag{30}$$

4.3. Calculation of Supporting Counterforce. According to the principle of virtual power,

$$W_{\text{ext}} = D_{\text{int}}. \tag{31}$$

The expression of surrounding rock pressure is

$$q = \frac{\gamma \cdot h \cdot (f_1 + f_2 + f_3 + f_4 + f_5) - c \cdot (f_7 + f_8 + f_9 + f_{10} + f_{11} + f_{12} + f_{13} + f_{14})}{f_6}. \tag{32}$$

Above all of the formulas, h is the height of the cavity, measured in meter. l represents the width of the cavity, measured in meter. q is the vertical supporting pressure, and e is the lateral supporting pressures of which the unit is kPa. φ is the internal friction angle, measured in degree. γ is the unit weight of soil, measured in kg/m^3. c is the cohesion, measured in kPa. K is the lateral pressure coefficient. V_0, V_1, V_2, V_3, and V_4 are the speed in the velocity field. α_1, α_2, α_3, and α_4 are the geometrical variables which determine the shape of the failure mechanism whose unit is degree. W is the external power, W_{exit} is the external total power, W_{soil} is the weight power of surrounding rock, W_T is the power of support of the antiforce, and the unit is watt. W_1, W_2, W_3, W_4, and W_5 are variables. D is the dissipation power of internal energy, and f_0, f_1, f_2, …, f_{14} are variables.

The constraint condition of Equation (32) is

$$\alpha_1 + \alpha_2 + \alpha_3 + \alpha_4 = \frac{\pi}{2} + \varphi_{t,} \tag{33}$$

Invoking the command in the Matlab software optimization toolbox, it will generate a set of angle data under the constraint condition (33). According to the formula of the surrounding rock pressure, an upper bound solution q is obtained; then, by adjusting the variable parameter values, numerous q values are obtained, in which the maximum q is the upper bound solution of the surrounding rock pressure.

5. Result Analysis

Under the nonlinear Hoek–Brown failure criterion, the upper bound theorem is used to analyze the influence of related parameters on the surrounding rock pressure of deep cavity. According to the failure mechanism and method mentioned above, the calculation results are as follows.

5.1. Influence of γ and K on Surrounding Rock Pressure. To investigate the influence of γ and K on the surrounding rock pressure, the parameters are assumed as follows: Cavity width l = 10 m, height h = 10 m, geological strength index GSI = 20, rock mass constant m_i = 20, uniaxial compressive strength σ_{ci} = 400 kPa, disturbance factor D = 0, and γ is the soil gravity, which had taken the values of 16, 18, 20, 22, 24, and 26 kN/m^3, respectively, in the experiment. Similarly, the coefficient K was taken 0.4, 0.6, 0.8, 1.0, 1.2, and 1.4, respectively. According to the failure mechanism constructed in this paper which combined translational destruction and rotational destruction together, the upper bound solution of the surrounding rock pressure obtained by the limit analysis method is shown in Tables 1 and 2 and Figures 4 and 5. The tables and figures present that the surrounding rock pressures q and e increase with the rising of soil gravity γ, and the pressure of surrounding rock q decreases, the surrounding rock pressure e increases with the rising of coefficient K. It shows that the buried depth has certain influence on the surrounding rock pressure.

The graph is drawn from the above table, as follows.

5.2. Influence of Chambers Section Size on Surrounding Rock Pressure. Likewise, to study the influence of chambers section size on the surrounding rock pressure, the parameters are soil gravity γ = 20 kN/m^3, coefficient K = 1.0, geological strength index GSI = 20, rock mass constant m_i = 20, uniaxial compressive strength σ_{ci} = 400 kPa, disturbance factor D = 0; the value of chamber width l and height h was taken as 5, 6, 7, 8, 9, and 10 m, respectively, in the experiment to conduct further analysis. According to the failure mechanism constructed in this paper which combined translational destruction and rotational destruction together, the upper bound solution of the surrounding rock pressure obtained by the limit analysis method is shown in Tables 3 and 4 and Figures 6 and 7. The tables and figures present that the surrounding rock pressures q and e increase with the rising of the chamber width l and height h, and the effect is obvious. Based on the research and above illustration, it is obvious that the chambers section size has a great influence on the pressure of surrounding rock.

5.3. Influence of GSI and m_i on Surrounding Rock Pressure. To study the influence of GSI and m_i on the surrounding rock pressure, the parameters are soil gravity γ = 20 kN/m^3, coefficient K = 1.0, cavity width l = 10 m, height h = 10 m, uniaxial compressive strength σ_{ci} = 400 kPa, disturbance factor D = 0, and the value of geological strength index GSI was taken as 10, 15, 20, 25, 30, and 35, respectively; rock mass constant value m_i was taken as 5, 10, 15, 20, 25, and 30, respectively. According to the failure mechanism constructed in this paper which combined translational destruction and rotational destruction, the upper bound solution of the surrounding rock pressure obtained by the limit analysis method is shown in Tables 5 and 6 and Figures 8 and 9.

The graph is drawn from the above table, as follows.

When coefficient K = 1.0, the surrounding rock pressure $e = q$. The tables and figures show that the surrounding rock pressure q and e decrease with the increasing of the geological strength index GSI and rock mass constant m_i, and the influence is apparent. It could be concluded that the

Table 1: Upper bound solution of the surrounding rock pressure q at different γ and K.

γ(kN/m^3)	q (kPa)					
	K = 0.4	K = 0.6	K = 0.8	K = 1.0	K = 1.2	K = 1.4
16	112.1	84.0	67.2	56.1	48.2	42.2
18	153.9	115.7	92.8	77.6	66.6	58.4
20	201.9	152.3	122.5	102.5	88.1	77.3
22	255.8	193.6	156.0	130.7	112.5	98.8
24	315.5	239.5	193.3	162.1	139.7	122.7
26	380.9	289.9	234.3	196.8	169.6	149.1

Table 2: Upper bound solution of the surrounding rock pressure e at different γ and K.

γ(kN/m^3)	e (kPa)					
	K = 0.4	K = 0.6	K = 0.8	K = 1.0	K = 1.2	K = 1.4
16	44.8	50.4	53.8	56.1	57.8	59.1
18	61.5	69.4	74.2	77.6	80.0	81.8
20	80.7	91.4	98.0	102.5	105.7	108.2
22	102.3	116.2	124.8	130.7	135.0	138.3
24	126.2	143.7	154.6	162.1	167.6	171.8
26	152.3	173.9	187.5	196.8	203.6	208.8

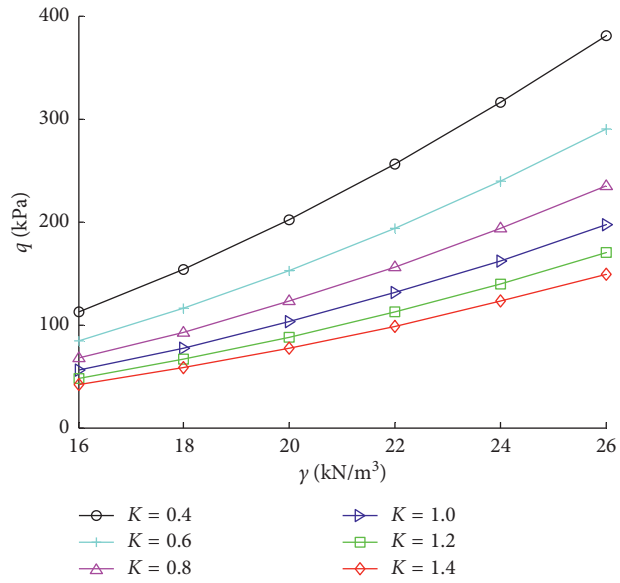

Figure 4: Effect of γ and K on the surrounding rock pressure q.

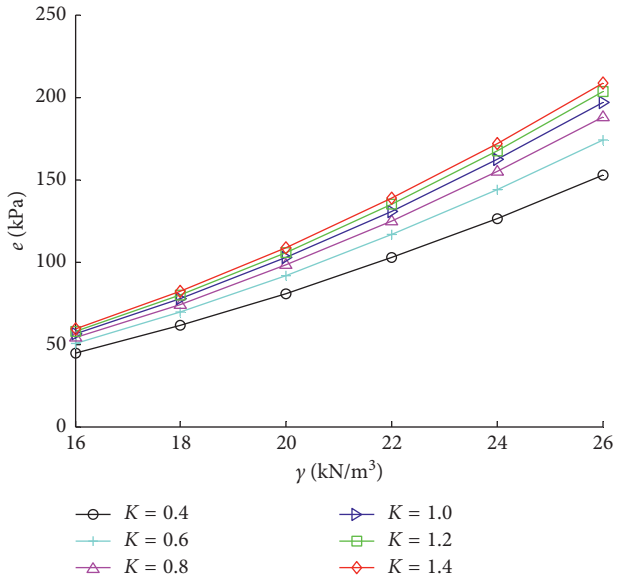

Figure 5: Effect of γ and K on the surrounding rock pressure e.

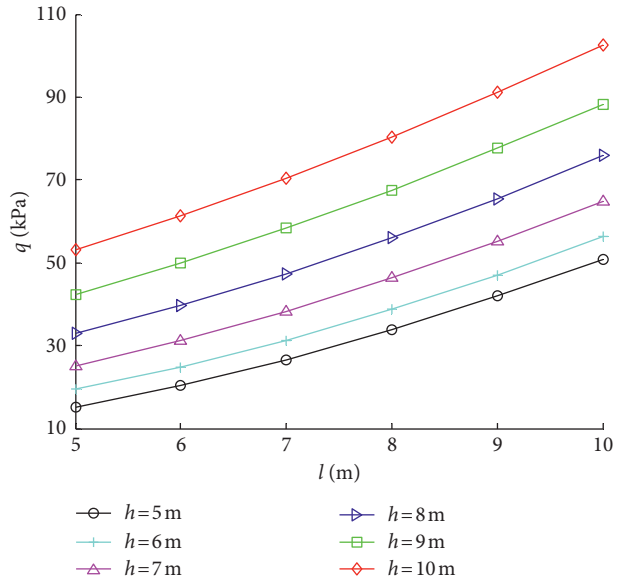

Figure 6: Effect of l and h on the surrounding rock pressure q.

Table 3: Upper bound solution of the surrounding rock pressure q at different l and h.

l (m)	q (kPa)					
	$h=5$ m	$h=6$ m	$h=7$ m	$h=8$ m	$h=9$ m	$h=10$ m
5	15.0	19.4	25.1	32.9	42.2	53.0
6	20.3	24.9	31.2	39.7	49.8	61.3
7	26.6	31.3	38.3	47.4	58.3	70.5
8	33.9	38.7	46.3	56.1	67.5	80.4
9	42.0	47.0	55.2	65.5	77.6	91.1
10	50.9	56.2	64.9	75.8	88.3	102.5

Table 4: Upper bound solution of the surrounding rock pressure e at different l and h.

l (m)	e (kPa)					
	$h=5$ m	$h=6$ m	$h=7$ m	$h=8$ m	$h=9$ m	$h=10$ m
5	15.0	19.4	25.1	32.9	42.2	53.0
6	20.3	24.9	31.2	39.7	49.8	61.3
7	26.6	31.3	38.3	47.4	58.3	70.5
8	33.9	38.7	46.3	56.1	67.5	80.4
9	42.0	47.0	55.2	65.5	77.6	91.1
10	50.9	56.2	64.9	75.8	88.3	102.5

The graph is drawn from the above table, as follows.

quality of surrounding would have a significant and direct influence on the pressure of surrounding rock.

5.4. Influence of σ_{ci} and D on Surrounding Rock Pressure. To study the influence of σ_{ci} and D on the surrounding rock pressure, the parameters are soil gravity $\gamma = 20$ kN/m^3, coefficient $K = 1.0$, cavity width $l = 10$ m, height $h = 10$ m, geological strength index GSI = 20, rock mass constant $m_i = 20$, uniaxial compressive strength had taken the value of 200, 400, 600, 800, 1000, and 1200 kPa, and the disturbance factor D had taken the value of 0, 0.2, 0.4, 0.6, 0.8, and 1.0, respectively, to conduct further analysis. According to the failure mechanism constructed in this paper which combined translational destruction and rotational

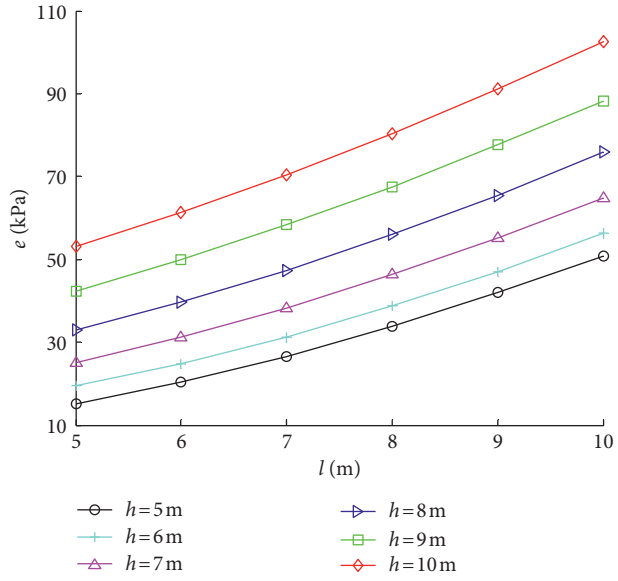

Figure 7: Effect of l and h on the surrounding rock pressure e.

Table 5: Upper bound solution of the surrounding rock pressure q at different GSI and m_i.

GSI	q (kPa)					
	$m_i=5$	$m_i=10$	$m_i=15$	$m_i=20$	$m_i=25$	$m_i=30$
10	1117.3	505.8	301.4	199.8	140.0	101.3
15	896.2	394.9	227.7	145.3	97.5	67.4
20	718.9	306.0	169.0	102.5	64.9	43.4
25	575.5	234.2	122.2	69.2	41.7	25.0
30	458.6	176.1	85.1	40.7	27.3	16.1
35	362.6	129.0	56.2	29.3	15.5	6.7

Table 6: Upper bound solution of the surrounding rock pressure e at different GSI and m_i.

GSI	e (kPa)					
	$m_i = 5$	$m_i = 10$	$m_i = 15$	$m_i = 20$	$m_i = 25$	$m_i = 30$
10	1117.3	505.8	301.4	199.8	140.0	101.3
15	896.2	394.9	227.7	145.3	97.5	67.4
20	718.9	306.0	169.0	102.5	64.9	43.4
25	575.5	234.2	122.2	69.2	41.7	25.0
30	458.6	176.1	85.1	40.7	27.3	16.1
35	362.6	129.0	56.2	29.3	15.5	6.7

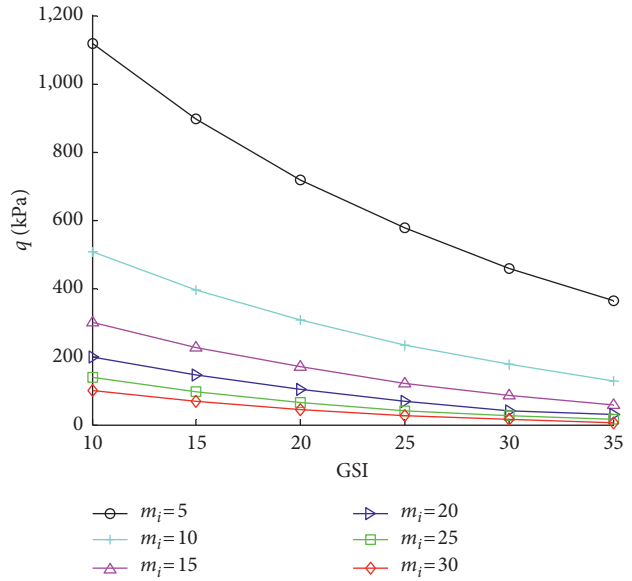

Figure 8: Effect of GSI and m_i on the surrounding rock pressure q.

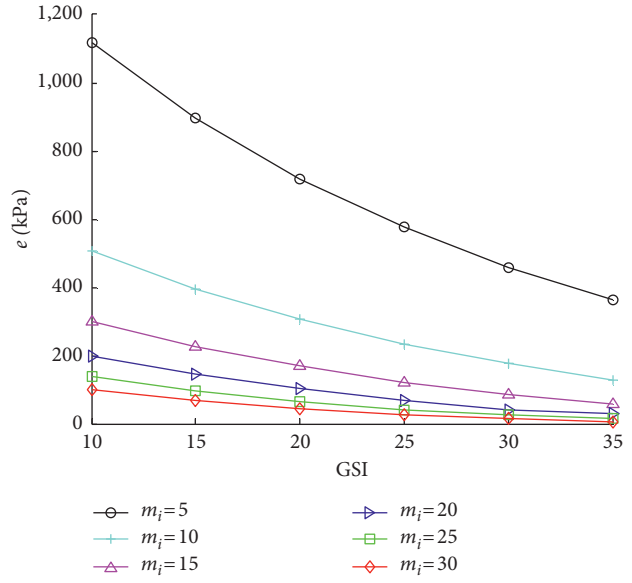

Figure 9: Effect of GSI and m_i on the surrounding rock pressure e.

destruction, the upper bound solution of the surrounding rock pressure obtained by the limit analysis method is shown in Tables 7 and 8 and Figures 10 and 11.

Table 7: Upper bound solution of the surrounding rock pressure q at different σ_{ci} and D.

σ_{ci} (kPa)	q (kPa)					
	$D = 0$	$D = 0.2$	$D = 0.4$	$D = 0.6$	$D = 0.8$	$D = 1.0$
200	262.5	400.6	647.8	1148.6	2366.8	6292.6
400	102.5	177.2	314.9	595.8	1278.2	3473.7
600	49.9	98.1	193.5	393.1	879.8	2443.0
800	30.0	59.2	130.4	285.7	668.5	1897.5
1000	18.0	39.6	92.2	218.8	536.2	1556.1
1200	12.0	25.5	67.1	173.0	445.0	1320.9

Table 8: Upper bound solution of the surrounding rock pressure e at different σ_{ci} and D.

σ_{ci} (kPa)	e (kPa)					
	$D = 0$	$D = 0.2$	$D = 0.4$	$D = 0.6$	$D = 0.8$	$D = 1.0$
200	262.5	400.6	647.8	1148.6	2366.8	6292.6
400	102.5	177.2	314.9	595.8	1278.2	3473.7
600	49.9	98.1	193.5	393.1	879.8	2443.0
800	30.0	59.2	130.4	285.7	668.5	1897.5
1000	18.0	39.6	92.2	218.8	536.2	1556.1
1200	12.0	25.5	67.1	173.0	445.0	1320.9

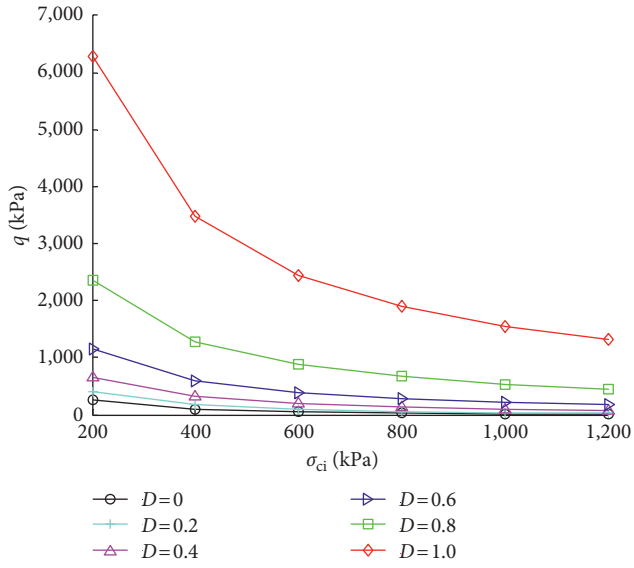

Figure 10: Effect of σ_{ci} and D on the surrounding rock pressure q.

The graph is drawn from the above table, as follows.

When coefficient K = 1.0, the surrounding rock pressure $e = q$. The tables and figures show that the surrounding rock pressure q and e decrease with the increasing of the uniaxial compressive strength σ_{ci}, while the surrounding rock pressure q and e increase with the rising of disturbance factor D. And the effect is obvious, which reveals that the disturbance factor would influence the pressure of surrounding rock directly.

6. Conclusion

(1) The nonlinear Hoek–Brown failure criterion is applied to the upper bound of limit analysis by the

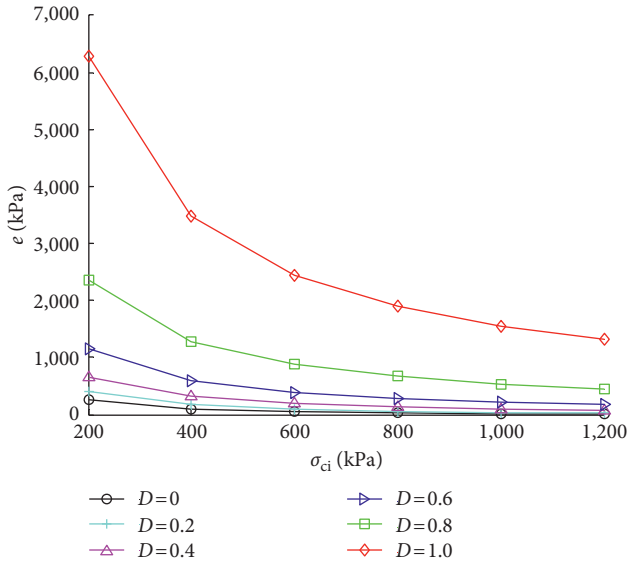

Figure 11: Effect of σ_{ci} and D on surrounding rock pressure e.

tangent method to construct the circular arc failure mechanism of deep cavity. According to the principle of virtual power, the analytic expression of surrounding rock pressure could be deduced, and the upper bound solution of the surrounding rock pressure of deep cavity could be obtained.

(2) The surrounding rock pressures increase obviously with the rising of soil gravity γ, tunnel width l, and tunnel height h. Besides, the pressure of surrounding rock q decreases with the rising of coefficient K, whereas the change rule of the surrounding rock pressure e is quite the opposite.

(3) The surrounding rock pressures decrease significantly with the increase of GSI, m_i and σ_{ci}, while the surrounding rock pressure increase greatly with the rising of D.

Data Availability

The data used to support the findings of this study are available from the corresponding author upon request.

Conflicts of Interest

The authors declare that they have no conflicts of interest.

Acknowledgments

The preparation of the paper has received financial support from the Key Program of the National Natural Science Foundation of China (51434006) and the National Natural Science Foundation of China (51538009, 51674115, 51804113). The financial support are greatly appreciated.

References

[1] D. B. Zhang, *Upper Bound Solutions of Earth Pressure and Structure System Reliability for Deep Cavity*, Central South University, Changsha, China, 2014.

[2] C. B. Qin, S. C. Chian, X. L. Yang, and D. C. Du, "2D and 3D limit analysis of progressive collapse mechanism for deep-buried tunnels under the condition of varying water table," *International Journal of Rock Mechanics and Mining Sciences*, vol. 80, pp. 255–264, 2015.

[3] J. H. Zhang, J. S. Xu, and B. Zhang, "Energy analysis of stability of twin shallow tunnels based on nonlinear failure criterion," *Journal of Central South University*, vol. 21, no. 12, pp. 4669–4676, 2014.

[4] Q. J. Pan and D. Dias, "The effect of pore water pressure on tunnel face stability," *International Journal for Numerical and Analytical Methods in Geomechanics*, vol. 40, no. 15, pp. 2123–2136, 2016.

[5] W. F. Chen, *Limit Analysis and Soil Plasticity*, J. Ross Publishing, Inc., Fort Lauderdale, FL, USA, 2007.

[6] E. H. Davis, M. J. Gunn, R. J. Mair, and H. N. Seneviratine, "The stability of shallow tunnels and underground openings in cohesive material," *Geotechnique*, vol. 30, no. 4, pp. 397–416, 1980.

[7] J. Takemura, T. Kimura, and S. F. Wong, "Undrained stability of two-dimensional unlined tunnels in soft soil," in *Proceedings of JSCE on Geotechnical Engineering*, No. 418/III-12, pp. 267–277, 1990.

[8] F. Yang and J. S. Yang, "Limit analysis method for determination of earth pressure on shallow tunnel," *Engineering Mechanics*, vol. 2, no. 7, pp. 179–184, 2008.

[9] J. H. Atkinson and D. M. Potts, "Stability of a shallow circular tunnel in cohesionless soil," *Geotechnique*, vol. 27, no. 2, pp. 203–215, 1977.

[10] M. Fraldi and F. Guarracino, "Limit analysis of collapse mechanisms in cavities and tunnels according to the Hoek-Brown failure criterion," *International Journal of Rock Mechanics and Mining Sciences*, vol. 46, no. 4, pp. 665–673, 2009.

[11] M. Fraldi and F. Guarracino, "Analytical solutions for collapse mechanisms in tunnels with arbitrary cross sections," *International Journal of Solids and Structures*, vol. 47, no. 2, pp. 216–223, 2010.

[12] M. Fraldi and F. Guarracino, "Evaluation of impending collapse in circular tunnels by analytical and numerical approaches," *Tunnelling and Underground Space Technology*, vol. 26, no. 4, pp. 507–516, 2011.

[13] F. Huang, D. B. Zhang, Z. B. Sun, and B. Wu, "Influence of pore water pressure on upper bound analysis of collapse shape for square tunnel in Hoek-Brown media," *Journal of Central South University of Technology*, vol. 18, no. 2, pp. 530–535, 2011.

[14] F. Rojat, V. Labiouse, and P. Mestat, "Improved analytical solutions for the response of underground excavations in rock masses satisfying the generalized Hoek-Brown failure criterion," *International Journal of Rock Mechanics and Mining Sciences*, vol. 79, no. 2, pp. 193–204, 2015.

[15] X. L. Yang and Z. X. Long, "Seismic and static 3D stability of two-stage rock slope based on Hoek-Brown failure criterion," *Canadian Geotechnical Journal*, vol. 53, no. 3, pp. 551–558, 2016.

[16] X. L. Yang, J. S. Xu, Y. X. Li, and R. M. Yan, "Collapse mechanism of tunnel roof considering joined influences of nonlinearity and non-associated flow rule," *Geomechanics and Engineering*, vol. 10, no. 1, pp. 21–35, 2016.

[17] F. Huang and X. L. Yang, "Upper bound limit analysis of collapse shape for circular tunnel subjected to pore pressure based on the Hoek-Brown failure criterion," *Tunnellingand Underground Space Technology*, vol. 26, no. 5, pp. 614–618, 2011.

[18] X. L. Yang and F. Huang, "Three-dimensional failure mechanism of a rectangular cavity in a Hoek-Brown rock medium," *International Journal of Rock Mechanics and Mining Sciences*, vol. 61, no. 10, pp. 189–195, 2013.

[19] C. Y. Han, J. J. Chen, X. H. Xia, and J. H. Wang, "Three-dimensional stability analysis of anisotropic and non-homogeneous slopes using limit analysis," *Journal of Central South University*, vol. 21, no. 3, pp. 1142–1147, 2014.

[20] X. L. Yang and F. Huang, "Collapse mechanism of shallow tunnel based on nonlinear Hoek-Brown failure criterion," *Tunneling and Underground Space Technology*, vol. 26, no. 6, pp. 686–691, 2011.